

Photoproduction of J/ψ Mesons at HERA

H1 Collaboration

Abstract

We present a study of J/ψ meson production in collisions of 26.7 GeV electrons with 820 GeV protons, performed with the H1-detector at the HERA collider at DESY. The J/ψ mesons are detected via their leptonic decays both to electrons and muons. Requiring exactly two particles in the detector, a cross section of $\sigma(ep \rightarrow J/\psi X) = (8.8 \pm 2.0 \pm 2.2)$ nb is determined for $30 \text{ GeV} \leq W_{\gamma p} \leq 180 \text{ GeV}$ and $Q^2 \lesssim 4 \text{ GeV}^2$. Using the flux of quasi-real photons with $Q^2 \lesssim 4 \text{ GeV}^2$, a total photoproduction cross section of $\sigma(\gamma p \rightarrow J/\psi X) = (56 \pm 13 \pm 14)$ nb is derived at an average $W_{\gamma p} = 90 \text{ GeV}$. The distribution of the squared momentum transfer t from the proton to the J/ψ can be fitted using an exponential $\exp(-b|t|)$ below a $|t|$ of 0.75 GeV^2 yielding a slope parameter of $b = (4.7 \pm 1.9) \text{ GeV}^{-2}$.

T. Ahmed³, S. Aid¹³, V. Andreev²⁴, B. Andrieu²⁸, R.-D. Appuhn¹¹, M. Arpagaus³⁶, A. Babaev²⁶,
 J. Baehr³⁵, J. Bán¹⁷, P. Baranov²⁴, E. Barrelet²⁹, W. Bartel¹¹, M. Barth⁴, U. Bassler²⁹, H.P. Beck³⁷,
 H.-J. Behrend¹¹, A. Belousov²⁴, Ch. Berger¹, H. Bergstein¹, G. Bernardi²⁹, R. Bernet³⁶,
 G. Bertrand-Coremans⁴, M. Besançon⁹, R. Beyer¹¹, P. Biddulph²², J.C. Bizot²⁷, V. Blobel¹³,
 K. Borrás⁸, F. Botterweck⁴, V. Boudry²⁸, A. Braemer¹⁴, F. Brasse¹¹, W. Braunschweig¹,
 V. Brisson²⁷, D. Bruncko¹⁷, C. Brune¹⁵, R. Buchholz¹¹, L. Büngener¹³, J. Bürger¹¹, F.W. Büsler¹³,
 A. Buniatian^{11,39}, S. Burke¹⁸, G. Buschhorn²⁶, A.J. Campbell¹¹, T. Carli²⁶, F. Charles¹¹, D. Clarke⁵,
 A.B. Clegg¹⁸, M. Colombo⁸, J.G. Contreras⁸, J.A. Coughlan⁵, A. Courau²⁷, Ch. Coutures⁹,
 G. Cozzika⁹, L. Criegee¹¹, D.G. Cussans⁵, J. Cvach³⁰, S. Dagoret²⁹, J.B. Dainton¹⁹, M. Danilov²³,
 W.D. Dau¹⁶, K. Daum³⁴, M. David⁹, E. Deffur¹¹, B. Delcourt²⁷, L. Del Buono²⁹, A. De Roeck¹¹,
 E.A. De Wolf⁴, P. Di Nezza³², C. Dollfus³⁷, J.D. Dowell³, H.B. Dreis², J. Duboc²⁹, D. Düllmann¹³,
 O. Dünger¹³, H. Duhm¹², J. Ebert³⁴, T.R. Ebert¹⁹, G. Eckerlin¹¹, V. Efremenko²³, S. Egli³⁷,
 H. Ehrlichmann³⁵, S. Eichenberger³⁷, R. Eichler³⁶, F. Eisele¹⁴, E. Eisenhandler²⁰, R.J. Ellison²²,
 E. Elsen¹¹, M. Erdmann¹⁴, W. Erdmann³⁶, E. Evrard⁴, L. Favart⁴, A. Fedotov²³, D. Feeken¹³,
 R. Felst¹¹, J. Feltesse⁹, J. Ferencei¹⁵, F. Ferrarotto³², K. Flamm¹¹, M. Fleischer¹¹, M. Flieser²⁶,
 G. Flügge², A. Fomenko²⁴, B. Fominykh²³, M. Forbush⁷, J. Formánek³¹, J.M. Foster²², G. Franke¹¹,
 E. Fretwurst¹², E. Gabathuler¹⁹, K. Gabathuler³³, K. Gamberding²⁶, J. Garvey³, J. Gayler¹¹,
 M. Gebauer⁸, A. Gellrich¹³, H. Genzel¹, R. Gerhards¹¹, U. Goerlach¹¹, L. Goerlich⁶, N. Gogitidze²⁴,
 M. Goldberg²⁹, D. Goldner⁸, B. Gonzalez-Pineiro²⁹, A.M. Goodall¹⁹, I. Gorelov²³, P. Goritchev²³,
 C. Grab³⁶, H. Grässler², R. Grässler², T. Greenshaw¹⁹, G. Grindhammer²⁶, A. Gruber²⁶,
 C. Gruber¹⁶, J. Haack³⁵, D. Haidt¹¹, L. Hajduk⁶, O. Hamon²⁹, M. Hampel¹, E.M. Hanlon¹⁸,
 M. Hapke¹¹, W.J. Haynes⁵, J. Heatherington²⁰, V. Hedberg²¹, G. Heinzelmänn¹³,
 R.C.W. Henderson¹⁸, H. Henschel³⁵, R. Herma¹, I. Herynek³⁰, M.F. Hess²⁶, W. Hildesheim¹²,
 P. Hill⁵, K.H. Hiller³⁵, C.D. Hilton²², J. Hladký³⁰, K.C. Hoeger²², M. Höppner⁸, R. Horisberger³³,
 Ph. Huet⁴, H. Hufnagel¹⁴, M. Ibbotson²², H. Itterbeck¹, M.-A. Jabiol⁹, A. Jacholkowska²⁷,
 C. Jacobsson²¹, M. Jaffre²⁷, J. Janoth¹⁵, T. Jansen¹¹, L. Jönsson²¹, K. Johannsen¹³, D.P. Johnson⁴,
 L. Johnson¹⁸, H. Jung¹¹, P.I.P. Kalmus²⁰, D. Kant²⁰, R. Kaschowitz², P. Kasselmann¹²,
 U. Kathage¹⁶, H.H. Kaufmann³⁵, S. Kazarian¹¹, I.R. Kenyon³, S. Kermiche²⁷, C. Keuker¹,
 C. Kiesling²⁶, M. Klein³⁵, C. Kleinwort¹³, G. Knies¹¹, W. Ko⁷, T. Köhler¹, H. Kolanoski⁸, F. Kole⁷,
 S.D. Kolya²², V. Korbel¹¹, M. Korn⁸, P. Kostka³⁵, S.K. Kotelnikov²⁴, M.W. Krasny^{6,29},
 H. Krehbiel¹¹, D. Krücker², U. Krüger¹¹, U. Krüner-Marquis¹¹, J.P. Kubenka²⁶, H. Küster²,
 M. Kuhlen²⁶, T. Kurča¹⁷, J. Kurzhöfer⁸, B. Kuznik³⁴, D. Lacour²⁹, F. Lamarche²⁸, R. Lander⁷,
 M.P.J. Landon²⁰, W. Lange³⁵, P. Lanus²⁶, J.-F. Laporte⁹, A. Lebedev²⁴, C. Leverenz¹¹,
 S. Levonian^{11,24}, Ch. Ley², A. Lindner⁸, G. Lindström¹², F. Linsel¹¹, J. Lipinski¹³, B. List¹¹,
 P. Loch²⁷, H. Lohmander²¹, G.C. Lopez²⁰, D. Lüke^{8,11}, N. Magnussen³⁴, E. Malinowski²⁴, S. Mani⁷,
 R. Maraček¹⁷, P. Marage⁴, J. Marks²⁵, R. Marshall²², J. Martens³⁴, R. Martin¹⁹, H.-U. Martyn¹,
 J. Martyniak⁶, S. Masson², T. Mavroidis²⁰, S.J. Maxfield¹⁹, S.J. McMahon¹⁹, A. Mehta²²,
 K. Meier¹⁵, D. Mercer²², T. Merz¹¹, C.A. Meyer³⁷, H. Meyer³⁴, J. Meyer¹¹, S. Mikocki⁶,
 D. Milstead¹⁹, F. Moreau²⁸, J.V. Morris⁵, G. Müller¹¹, K. Müller³⁷, P. Murín¹⁷, V. Nagovizin²³,
 R. Nahnauer³⁵, B. Naroska¹³, Th. Naumann³⁵, P.R. Newman³, D. Newton¹⁸, D. Neyret²⁹,
 H.K. Nguyen²⁹, F. Niebergall¹³, C. Niebuhr¹¹, R. Nisius¹, G. Nowak⁶, G.W. Noyes⁵,
 M. Nyberg-Werther²¹, H. Oberlack²⁶, U. Obrock⁸, J.E. Olsson¹¹, E. Panaro¹², A. Panitch⁴,
 C. Pascaud²⁷, G.D. Patel¹⁹, E. Peppel¹¹, E. Perez⁹, J.P. Phillips²², Ch. Pichler¹², D. Pitzl³⁶,
 G. Pope⁷, S. Prell¹¹, R. Prosi¹¹, G. Rädcl¹¹, F. Raupach¹, P. Reimer³⁰, S. Reinshagen¹¹,
 P. Ribarics²⁶, V. Riech¹², J. Riedlberger³⁶, S. Riess¹³, M. Rietz², S.M. Robertson³, P. Robmann³⁷,
 H.E. Roloff³⁵, R. Roosen⁴, K. Rosenbauer¹, A. Rostovtsev²³, F. Rouse⁷, C. Royon⁹, K. Rüter²⁶,
 S. Rusakov²⁴, K. Rybicki⁶, R. Rylko²⁰, N. Sahlmann², E. Sanchez²⁶, D.P.C. Sankey⁵, M. Savitsky²³,
 P. Schacht²⁶, S. Schiek¹¹, P. Schleper¹⁴, W. von Schlippe²⁰, C. Schmidt¹¹, D. Schmidt³⁴,
 G. Schmidt¹³, A. Schöning¹¹, V. Schröder¹¹, E. Schuhmann²⁶, B. Schwab¹⁴, A. Schwind³⁵,
 U. Seehausen¹³, F. Sefkow¹¹, M. Seidel¹², R. Sell¹¹, A. Semenov²³, V. Shekelyan²³, I. Sheviakov²⁴,

H. Shooshari²⁶, L.N. Shtarkov²⁴, G. Siegmon¹⁶, U. Siewert¹⁶, Y. Sirois²⁸, I.O. Skillicorn¹⁰, P. Smirnov²⁴, J.R. Smith⁷, Y. Soloviev²⁴, H. Spitzer¹³, R. Starosta¹, M. Steenbock¹³, P. Steffen¹¹, R. Steinberg², B. Stella³², K. Stephens²², J. Stier¹¹, J. Stiewe¹⁵, U. Stösslein³⁵, J. Strachota³⁰, U. Straumann³⁷, W. Struczinski², J.P. Sutton³, S. Tapprogge¹⁵, R.E. Taylor^{38,27}, V. Tchernyshov²³, C. Thiebaux²⁸, G. Thompson²⁰, I. Tichomirov²³, P. Truöl³⁷, J. Turnau⁶, J. Tutas¹⁴, P. Uelkes², A. Usik²⁴, S. Valkár³¹, A. Valkárová³¹, C. Vallée²⁵, P. Van Esch⁴, P. Van Mechelen⁴, A. Vartapetian^{11,39}, Y. Vazdik²⁴, M. Vecko³⁰, P. Verrecchia⁹, G. Villet⁹, K. Wacker⁸, A. Wagener², M. Wagener³³, I.W. Walker¹⁸, A. Walther⁸, G. Weber¹³, M. Weber¹¹, D. Wegener⁸, A. Wegner¹¹, H.P. Wellisch²⁶, L.R. West³, S. Willard⁷, M. Winde³⁵, G.-G. Winter¹¹, A.E. Wright²², E. Wünsch¹¹, N. Wulff¹¹, T.P. Yiou²⁹, J. Žáček³¹, D. Zarbock¹², Z. Zhang²⁷, M. Zimmer¹¹, W. Zimmermann¹¹, F. Zomer²⁷, and K. Zuber¹⁵ ¹ I. Physikalisches Institut der RWTH, Aachen, Germany^a

² III. Physikalisches Institut der RWTH, Aachen, Germany^a

³ School of Physics and Space Research, University of Birmingham, Birmingham, UK^b

⁴ Inter-University Institute for High Energies ULB-VUB, Brussels; Universitaire Instellingen Antwerpen, Wilrijk, Belgium^c

⁵ Rutherford Appleton Laboratory, Chilton, Didcot, UK^b

⁶ Institute for Nuclear Physics, Cracow, Poland^d

⁷ Physics Department and IIRPA, University of California, Davis, California, USA^e

⁸ Institut für Physik, Universität Dortmund, Dortmund, Germany^a

⁹ CEA, DSM/DAPNIA, CE-SACLAY, Gif-sur-Yvette, France

¹⁰ Department of Physics and Astronomy, University of Glasgow, Glasgow, UK^b

¹¹ DESY, Hamburg, Germany^a

¹² I. Institut für Experimentalphysik, Universität Hamburg, Hamburg, Germany^a

¹³ II. Institut für Experimentalphysik, Universität Hamburg, Hamburg, Germany^a

¹⁴ Physikalisches Institut, Universität Heidelberg, Heidelberg, Germany^a

¹⁵ Institut für Hochenergiephysik, Universität Heidelberg, Heidelberg, Germany^a

¹⁶ Institut für Reine und Angewandte Kernphysik, Universität Kiel, Kiel, Germany^a

¹⁷ Institute of Experimental Physics, Slovak Academy of Sciences, Košice, Slovak Republic

¹⁸ School of Physics and Materials, University of Lancaster, Lancaster, UK^b

¹⁹ Department of Physics, University of Liverpool, Liverpool, UK^b

²⁰ Queen Mary and Westfield College, London, UK^b

²¹ Physics Department, University of Lund, Lund, Sweden^f

²² Physics Department, University of Manchester, Manchester, UK^b

²³ Institute for Theoretical and Experimental Physics, Moscow, Russia

²⁴ Lebedev Physical Institute, Moscow, Russia

²⁵ CPPM, Université d'Aix-Marseille II, IN2P3-CNRS, Marseille, France

²⁶ Max-Planck-Institut für Physik, München, Germany^a

²⁷ LAL, Université de Paris-Sud, IN2P3-CNRS, Orsay, France

²⁸ LPNHE, Ecole Polytechnique, IN2P3-CNRS, Palaiseau, France

²⁹ LPNHE, Universités Paris VI and VII, IN2P3-CNRS, Paris, France

³⁰ Institute of Physics, Czech Academy of Sciences, Praha, Czech Republic^g

³¹ Nuclear Center, Charles University, Praha, Czech Republic^g

³² INFN Roma and Dipartimento di Fisica, Università "La Sapienza", Roma, Italy

³³ Paul Scherrer Institut, Villigen, Switzerland

³⁴ Fachbereich Physik, Bergische Universität Gesamthochschule Wuppertal, Wuppertal, Germany^a

³⁵ DESY, Institut für Hochenergiephysik, Zeuthen, Germany^a

³⁶ Institut für Teilchenphysik, ETH, Zürich, Switzerland^h

³⁷ Physik-Institut der Universität Zürich, Zürich, Switzerland^h

³⁸ Stanford Linear Accelerator Center, Stanford California, USA

³⁹ Visitor from Yerevan Phys.Inst., Armenia

^a Supported by the Bundesministerium für Forschung und Technologie, FRG under contract numbers 6AC17P, 6AC47P, 6DO57I, 6HH17P, 6HH27I, 6HD17I, 6HD27I, 6KI17P, 6MP17I, and 6WT87P

^b Supported by the UK Particle Physics and Astronomy Research Council, and formerly by the UK Science and Engineering Research Council

^c Supported by FNRS-NFWO, IISN-IKW

^d Supported by the Polish State Committee for Scientific Research, grant No. 204209101

^e Supported in part by USDOE grant DE F603 91ER40674

^f Supported by the Swedish Natural Science Research Council

^g Supported by GA ČR, grant no. 202/93/2423 and by GA AV ČR, grant no. 19095

^h Supported by the Swiss National Science Foundation

1 Introduction

The investigation of the production of heavy quarks by real or virtual photons allows to probe strong interaction physics in a region of phase space which is characterised by a transition between the regime of perturbative QCD and the non-perturbative regime. Since the energy scale for the interaction is set by the mass of the heavy quark and thus is high enough to result in a sufficiently low value for the QCD coupling α_S , a perturbative approach is justified. On the other hand, perturbation theory breaks down if long range i.e. ‘soft’ interactions between heavy quarks and the proton dominate. The photoproduction of J/ψ vector mesons is ideal for studying this transition regime in the charm sector.

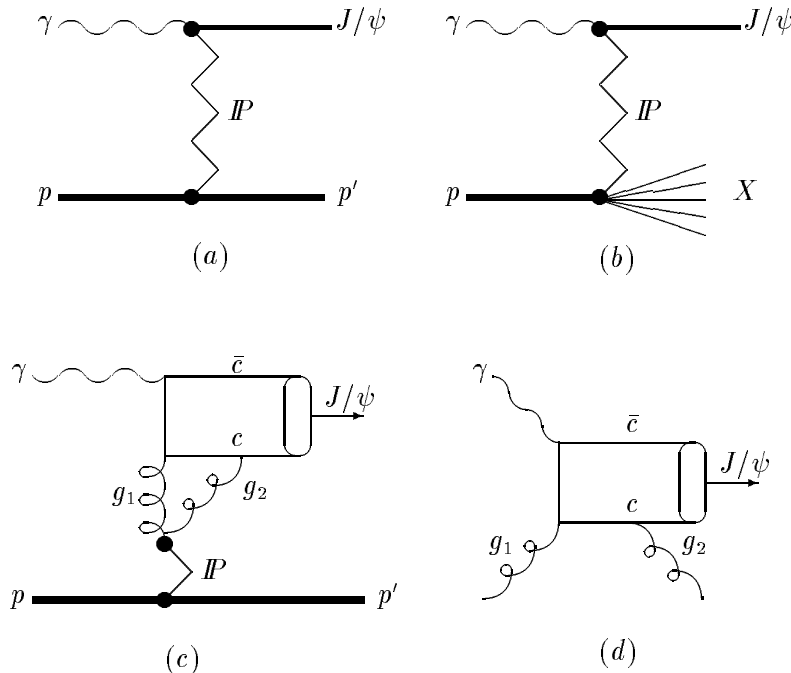


Figure 1: J/ψ production mechanisms: (a) Elastic J/ψ production via Pomeron exchange; (b) Diffractive proton dissociation; (c) Two Gluon Pomeron model for elastic J/ψ production [3]; (d) Photon Gluon Fusion model for inelastic J/ψ production (Colour-Singlet Model [4]).

Elastic and inelastic photoproduction of J/ψ mesons has been studied previously with virtual and real photons at center-of-mass energies $W_{\gamma p} \lesssim 30$ GeV [1]. At HERA the electron beam is a source of quasi-real photons and the energy range of such measurements can be considerably extended. The present study uses J/ψ events reconstructed by their leptonic decay. No particle in addition to the decay leptons is allowed in the detector. This type of event is expected to be produced via an elastic process as in figure 1a. Nevertheless a contamination from inelastic processes for instance from reactions where the proton breaks up and all proton fragments escape through the beampipe as in figure 1b cannot be avoided. Therefore, in addition to models for elastic scattering, models for inelastic J/ψ production have also to be considered in the description of the data.

A non-perturbative description of J/ψ meson production is given in the vector-meson-dominance model (VMD) [2], where the incident photon fluctuates into a virtual vector meson. Elastic and inelastic diffractive events are described by the interaction of the vector meson with the target proton via Pomeron exchange as indicated in figures 1a and b. The production cross section is expected to show all features of diffractive processes, e.g. a slow rise of the total cross section with energy and an exponential drop of the differential cross section with the squared momentum transfer t from the

proton to the J/ψ meson. Inelastic contributions in this description are due to processes with proton dissociation, which may lead to a faster rise of the cross section with energy and a smaller t -slope than in the elastic case [5].

In QCD and QCD inspired models J/ψ meson photoproduction can be interpreted as a fusion process between photons emitted by the electron and gluons from either the proton or from the Pomeron (figure 1c,d). A model for hard photon-gluon fusion processes is the colour-singlet model [4] of which there is an improved version by Jung et al. [3]. In this model the emission of a hard gluon emitted by the J/ψ constituents ensures that the J/ψ is in a colour-singlet state (figure 1d). This process leads in general to high multiplicity events but may look like elastic production if the J/ψ is produced with an energy close to the photon energy in the proton rest frame. In this approach the purely elastic contribution can be described by a fusion process between the photon and gluons emerging from the Pomeron (figure 1c).

The paper is organized as follows: After a brief description of the detector the event selection is described. It is followed by the determination of acceptance and selection efficiencies and results on the production cross section, the t distribution and an estimate of the $J/\psi p$ elastic cross section. Finally the results are compared with previous data and model predictions.

Preliminary results for J/ψ production were reported by the ZEUS and H1 collaborations in [6].

2 Experimental Setup

The measurement was performed using the H1-detector at the electron-proton storage ring HERA. The data corresponds to an integrated luminosity of 259 nb^{-1} (284 nb^{-1}) for the decays $J/\psi \rightarrow \mu^+ \mu^-$ ($e^+ e^-$), respectively. In 1993 HERA was operated with 84 colliding bunches of electrons and protons with energies of 26.7 and 820 GeV respectively. Electron and proton beams featured so-called pilot bunches, i.e. beam bunches with no corresponding collision partner in the other beam. They are used for background determination.

2.1 The H1-detector

A detailed description of the H1-detector has been given elsewhere [7]. Here, only the components essential for this particular analysis are described.

The present analysis is mainly based on the central tracking system covering polar angles between 20° and 160° ¹. It is mounted concentrically around the beamline inside a homogeneous magnetic field of 1.15 T. Measurements of charge and momenta of charged particles are provided by two cylindrical drift chambers (central jet chambers, CJC) [8], which yield up to 56 space points. Two sets of cylindrical drift chambers for measurement of the z -coordinate and multiwire proportional chambers for triggering are placed in two radial positions. One set surrounds the beampipe within the inner CJC and the other is mounted in between the two jet chambers. The central tracking system is complemented by a forward tracking system which covers polar angles below 20° . In the present analysis it is only used to veto events with tracks other than the J/ψ decay leptons.

All tracking detectors are surrounded by a highly segmented liquid argon sampling calorimeter [9], consisting of an inner electromagnetic section with lead absorber plates and an outer hadronic section with steel absorber plates. The total depth of the electromagnetic section is 20 to 30 radiation lengths, which provides a resolution (as measured in a test-beam) $\sigma/E \approx 12\%/\sqrt{E}$, where E is in GeV. Electron identification is based on the measurement of the longitudinal shower shape and a comparison of the calorimetric energy measurement with the corresponding track momentum. Polar

¹H1 uses a right-handed coordinate system defined as follows: the origin is at the interaction point with the z -axis pointing in the proton beam direction, hence the polar angle is measured with respect to the proton beam direction. The region of small polar angles is called “forward”. The y -axis points upwards.

angles between 4° and 153° are covered by the calorimeter. The combined thickness of both calorimeter sections varies between 4.5 and 8 interaction lengths depending on polar angle.

The iron yoke surrounding the superconducting solenoid is instrumented with limited streamer tubes to provide muon identification. The muon detector is subdivided into an octagonal “barrel” surrounding the tracking detectors and calorimeters, and “end-caps” which cover the forward and backward region. The barrel is further subdivided into 32 modules (2-fold in z , 16-fold in ϕ) and each end-cap is divided into 16 modules (2-fold in x , 8-fold in y). The iron yoke is segmented into 10 iron plates of 7.5 cm thickness and instrumented with 16 layers of streamer tubes. Five of these layers are equipped with strips perpendicular to the wire direction to measure the coordinate along the wire and the other 11 with large rectangular pads for a coarse energy measurement. Using the coordinates of the digitally read out wires and strips, and the pads to resolve ambiguities, muon track elements can be reconstructed in the region $4^\circ < \theta < 171^\circ$ with a spatial resolution of the order of 1 cm. Muons with momenta above $p_\mu \gtrsim 1.5$ GeV ($p_\mu \gtrsim 0.8$ GeV) can be detected in the forward and barrel (backward) part. For penetrating muons in the barrel region the detection efficiency is $\approx 90\%$ and limited by the geometrical acceptance.

The luminosity is measured using the radiative process $ep \rightarrow ep\gamma$ where both the photon and the scattered electron are detected in a luminosity monitor as described in [7].

2.2 Trigger

The triggering of events with a J/ψ meson in the final state is one of the challenges of the experiment. The J/ψ mesons accepted in the detector are predominantly produced with low transverse momenta and the transverse momenta of the decay leptons are of the order of half the J/ψ mass. The efficiency of the trigger provided by the muon detector is marginal at such low momenta and the calorimeter does not provide a trigger for particles with momenta below a few GeV.

Furthermore, the time between bunch crossings at HERA is only 96 nsec. In order to minimize dead time the first level trigger uses a pipeline which demands that the trigger decision be taken within $2.3 \mu\text{sec}$. Due to this time limitation only simple trigger elements can be used in the first level trigger.

The J/ψ decays into electrons are triggered by track triggers only, those decaying into muons are triggered by combinations of track and muon triggers.

The track triggers are derived from proportional chambers and from the CJC. The multiwire proportional chambers deliver fast information about the longitudinal (z -) vertex position of the tracks. For the z -vertex trigger [10] at least two tracks have to point to a z -region of approximately ± 50 cm around the nominal interaction point at $z = 0$ (the beam intersection region has a length of about ± 30 cm).

The drift chamber trigger [11] finds tracks in the two central drift chambers which have a distance of closest approach of less than 2 cm from the nominal beam axis. Therefore interactions of off-axis beam particles in the material of the beam pipe are suppressed. The trigger combination for $J/\psi \rightarrow e^+e^-$ decays requires track candidates in the central drift chamber trigger and a z -vertex trigger.

The muon trigger uses five of the 16 layers of the iron instrumentation. In the barrel part and the backward (forward) end-cap a signal from a minimum of three (four) out of the five possible planes is required in at least one module. This leads to an effective trigger threshold of 1.5 GeV. A typical trigger for $J/\psi \rightarrow \mu^+\mu^-$ decays is a combination of a muon trigger in either of the muon modules, a track found in the drift chamber trigger and a z -vertex trigger.

A veto by a time-of-flight system is included in the triggers which rejects proton beam induced background from upstream of the detector.

3 Data Analysis

3.1 Event Selection

The aim of the event selection is the identification of J/ψ mesons with subsequent leptonic decays and no additional particles. In order to control efficiencies, the event selection is carried out in several steps. In the first step, events with at least two tracks originating from the interaction region with transverse momenta $p_t > 200$ MeV and radial lengths of at least 15 cm are selected. For each track the point of closest approach to the primary vertex is calculated in the bending plane. The cut on its radial distance from the vertex is $d_{dca} < 2$ cm. The z -coordinate of the point of closest approach has to fulfil $|z_{dca}| < 50$ cm. In addition the two values of z_{dca} for the lepton pair candidates have to be within 15 cm of each other. These cuts suppress background from beam-gas interactions and proton scattering off the beampipe. Cosmic ray muons are recognized as two coplanar tracks without additional tracks in the event and are rejected.

The drift chamber tracks are identified as muon candidates if they can either be linked to track elements reconstructed in the muon detector or if they are identified as minimum ionizing particles in the liquid argon calorimeter. The latter method extends the muon identification down to momenta of about 0.8 GeV.

A drift chamber track is identified as an electron candidate if it is linked to an electromagnetic cluster in the liquid argon calorimeter. The minimum energy for a cluster to be accepted is 1 GeV, in addition an energy dependent upper cut on the longitudinal shower length is applied. The minimum transverse distance between the extrapolated track and the reconstructed cluster position at the entrance of the electromagnetic calorimeter is required to be less than 10 cm. The cluster energy is then compared with the momentum of the track and a cut of $E_{cluster}/p > 0.5$ is imposed. For the second electron the minimum energy requirement is relaxed to $E_{cluster} > 500$ MeV.

In the final step candidate events are selected by requiring that no tracks other than the decay leptons coming from the interaction point are visible in the tracking detectors, that is in a region of $7^\circ \leq \theta \leq 170^\circ$. This last step is verified by a visual scan of the events in which events with an energy deposit above noise in the calorimeter in addition to the signals of the decay leptons are also rejected.

The final sample of two lepton events consists of 48 muon pair and 40 electron pair candidates with an invariant mass of the lepton pair $m_{l+l-} > 1.5$ GeV and both leptons in the acceptance region $20^\circ \leq \theta \leq 160^\circ$. In calculating the invariant mass m_{l+l-} the precisely known (x, y) -coordinates of the beam spot are used as an additional constraint as well as the requirement of a common origin in z . The mass distribution of the lepton pairs is shown in figure 2. A clear peak is observed at a mass of 3.10 GeV with a width of $\sigma = 0.12$ GeV. The numbers are from a fit of a Gaussian including a linear background term to the data in the J/ψ mass region. The background below the J/ψ peak is seen to be small (figure 2) and can be explained by lepton pairs produced in photon-photon scattering (see next section).

In a region of ± 225 MeV around the nominal J/ψ mass of 3.10 GeV, 22 muon pair events and 10 electron pair events are found. Since the scattered electron is not registered, i.e. its polar angle is $\theta \gtrsim 176^\circ$, the events have $Q^2 \lesssim 4$ GeV², where Q^2 is the momentum transfer squared of the scattered electron.

3.2 Acceptance and Detection Efficiency

In order to determine the acceptance and the efficiencies of the trigger and event selection Monte Carlo techniques are used. Events are generated according to the different models and the detector response is simulated in detail. The simulated events are subjected to the same reconstruction and analysis chain as the data.

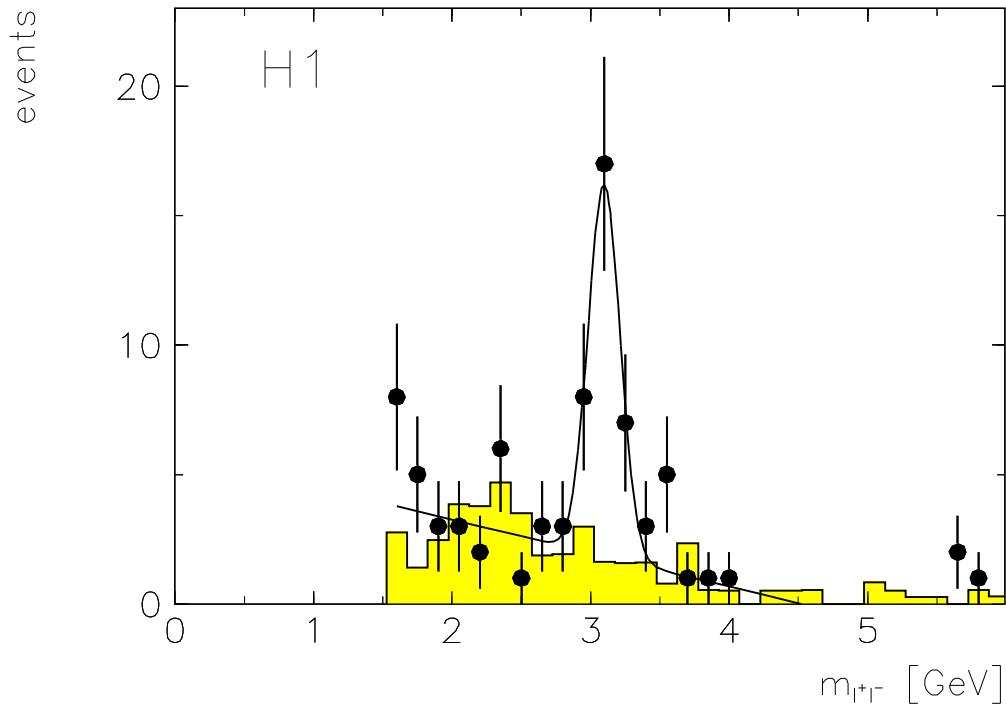


Figure 2: Mass distribution for $ep \rightarrow \ell^+\ell^- + X$ above 1.5 GeV . The curve is a fit of a Gaussian plus a linear background to the J/ψ mass region. The shaded histogram shows the contribution of QED lepton pairs.

The diffractive J/ψ production mechanism in the VMD model is used as simulated in the program PYTHIA [12] with a photon spectrum as described in [13]. The default setting of the PYTHIA generator gives at HERA energy a mixture of approximately 50% elastic events and 50% events with single diffractive proton dissociation. The distribution of data and diffractive Monte Carlo as a function of photon proton cms energy is shown in figure 3, the average energy is $W_{\gamma p} \approx 90\text{ GeV}$.

The geometrical acceptance for J/ψ meson production is found to be 0.63 ± 0.04 if both leptons are required to be within the acceptance region of $20^\circ \leq \theta \leq 160^\circ$. This value is valid for $Q^2 \leq 4\text{ GeV}^2$ and for $30\text{ GeV} \leq W_{\gamma p} \leq 180\text{ GeV}$, where $W_{\gamma p}$ is the total photon proton center-of-mass energy. The acceptance is nearly independent of the model for the present two-prong event selection. The small variations of the acceptance due to model variations (e.g. elastic versus inelastic and VMD versus QCD model) is 6% and is included in the systematic error given above. Further contributions to the systematic error of the acceptance are due to uncertainties in the angular distribution of the decay leptons (2%), and uncertainties in the energy dependence of the cross section (2%) in the accepted range.

The main contribution to the background is from QED lepton pair production by two virtual photons, where one photon is emitted from the incident electron and the other from the proton. For elastic production (where the proton remains intact) the dipole form factor and for the inelastic process the form factors given in [14] and [15] are used in the calculation. The accepted QED lepton pair background normalized to the luminosity is shown in figure 2. The number of QED events below the J/ψ peak is estimated to be 3 for each decay channel.

The efficiencies for the selection cuts deduced from the simulation are shown in table 1. Detailed checks were made using independent data samples to assess the ability of the detector simulation to describe the data quantitatively, only the most important of which will be discussed here. These checks cannot be performed for the complete phase space, therefore the Monte Carlo simulation has to be used for calculating the cross section.

	$J/\psi \rightarrow e^+e^-$	$J/\psi \rightarrow \mu^+\mu^-$
Track Reconstruction for 2 tracks	0.87±0.10	
Pair Identification	0.82±0.05	0.76±0.08
Selection Cuts	0.83±0.03	0.86±0.03
Trigger Efficiency	0.16±0.025	0.34±0.05
Total Selection Efficiency	0.095±0.02	0.193±0.04
# Events (background subtracted)	7±3	19±5
$\int Ldt$ [nb ⁻¹]	284	259
$\sigma(ep \rightarrow J/\psi + X \rightarrow \ell^+\ell^- + X)_{acc}$ [nb]	0.259±0.124	0.380 ± 0.096
Average σ_{acc} [nb]	0.334 ± 0.075	

Table 1: *Efficiencies and cross sections for J/ψ detection in the acceptance region (the decay leptons within $20^\circ \leq \theta \leq 160^\circ$) are given in the upper and lower part of the table, respectively. Efficiencies are calculated using the elastic VMD model with full detector simulation. The efficiency errors are systematic while the errors in the lower part of the table are purely statistical.*

The efficiency of the various components contributing to the triggers is estimated from the data using redundant triggers. The performance of the track and muon triggers in particular is verified using events triggered by the calorimeter. The average track reconstruction efficiency is determined from cosmic ray muons. The muon identification efficiency depends on momentum and polar angle and is also verified using cosmic ray muons. The electron identification efficiency is checked by selecting delta electrons produced by cosmic ray muons in the detector.

The agreement between data and simulation in these independent data samples is in all cases better than 10% and in most cases of the order of a few percent. The deviation between experimental efficiency and the corresponding simulated number can be regarded as a measure of the systematic error. The systematic errors of the efficiencies derived in this way are given in the first part of table 1. Adding the contributions in quadrature results in a total detection efficiency in the acceptance region of 0.095 for electron pairs and 0.19 for muon pairs with a systematic error of 22%.

4 Results

Using the number of events, the detection efficiencies and the integrated luminosity indicated in table 1, the cross sections for J/ψ production with subsequent decay into e^+e^- and $\mu^+\mu^-$ are computed for the given kinematical region and are listed in table 1. Since both measurements agree within statistical errors the weighted average is calculated. After acceptance correction and taking into account a branching ratio for J/ψ decay into lepton pairs of 0.060 ± 0.003 [16] the following cross section results:

$$\sigma(ep \rightarrow J/\psi + X) = (8.8 \pm 2.0 \pm 2.2) \text{ nb.}$$

The cross section is valid for $Q^2 < 4 \text{ GeV}^2$ and $30 \text{ GeV} < W_{\gamma p} < 180 \text{ GeV}$ at an ep center-of-mass energy of $\sqrt{s} = 296 \text{ GeV}$ for J/ψ s with no additional particles in a range of polar angles between 7° and 170° . The first error of the cross section is statistical, the second is due to systematic uncertainties. The main contributions to the systematic error come from the trigger and detection efficiency (22%, table 1), QED background subtraction (8%), luminosity determination (5%), acceptance (6%) and decay branching ratio (4%). Adding these in quadrature a total systematic error of $\approx 25\%$ results. Note that a contribution from cascade decays of $\psi' \rightarrow J/\psi + \text{neutrals}$ is not corrected for since it is estimated to be of the order of one event. Contributions to the J/ψ signal from other sources,

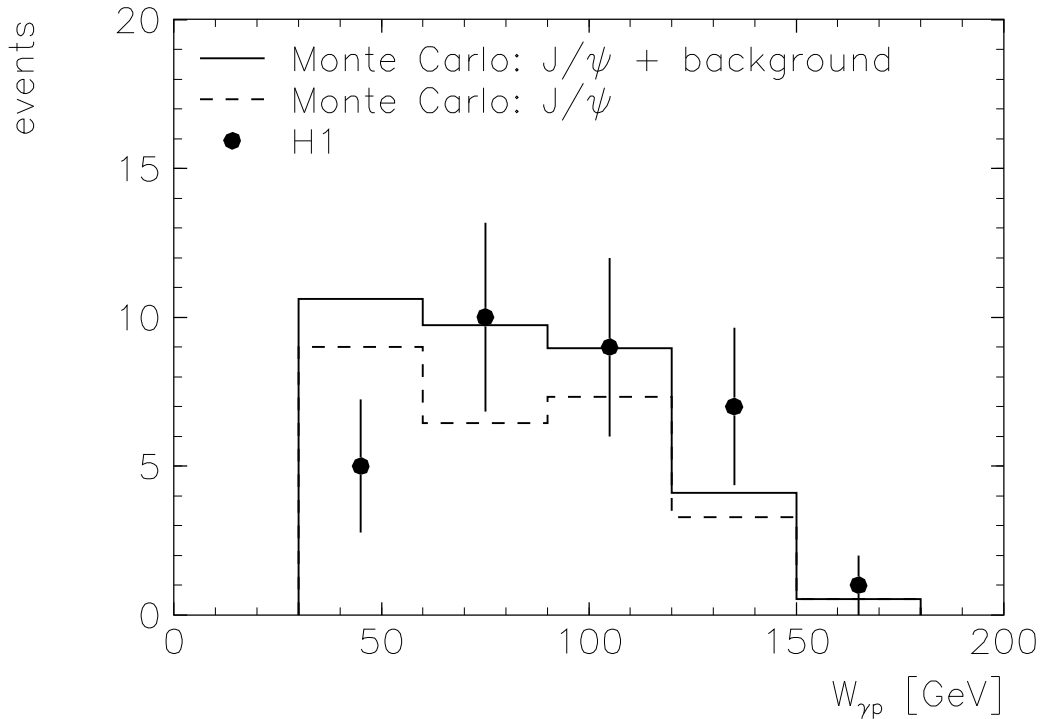


Figure 3: Center-of-mass energy of the photon proton system for the J/ψ candidate events. The histograms show the Monte Carlo simulations including detector effects. The dashed histogram shows the contribution from J/ψ production (VMD model PYTHIA) normalized to the data in the J/ψ mass region. In the full histogram the background from two-photon lepton pairs is included.

e.g. decays of the b quark or resolved photon processes are estimated to yield a negligible background ($< 10^{-3}$) [17].

The ep cross section can be converted into a γp cross section using the relation:

$$\sigma(ep \rightarrow J/\psi + X) = \int_{y_{min}}^{y_{max}} dy \int_{Q_{min}^2(y)}^{Q_{max}^2} dQ^2 \cdot f_{\gamma/e}(y, Q^2) \cdot \sigma(\gamma p \rightarrow J/\psi + X),$$

where

$$f_{\gamma/e}(y, Q^2) = \frac{\alpha}{2\pi} \frac{1}{y Q^2} \cdot [1 + (1 - y)^2 - \frac{2m_e^2 y^2}{Q^2}] \quad \text{with} \quad y = \frac{W_{\gamma p}^2 + Q^2 - m_p^2}{s}$$

is the flux of transverse photons [13]; $\sqrt{s} = 296$ GeV denotes the ep center-of-mass energy, $Q_{max}^2 = 4$ GeV². Due to the $1/Q^2$ dependence the dominant contribution to the photon flux is at small Q^2 (the average Q^2 is 10^{-3} GeV²). Therefore the dependence of the γp cross section on Q^2 can be neglected to obtain the cross section at $Q^2 = 0$. Assuming a VMD propagator using the J/ψ -mass the resulting error is less than a percent for the given Q_{max}^2 . Assuming $\sigma(\gamma p)$ to be independent of the photon energy the integral of $f_{\gamma/e}(y, Q^2)$ is calculated to be 0.158 in an interval of 30 GeV $\leq W_{\gamma p} \leq 180$ GeV for a maximum $Q_{max}^2 = 4$ GeV².

A total photoproduction cross section of

$$\sigma(\gamma p \rightarrow J/\psi + X) = (56 \pm 13 \pm 14) \text{ nb}$$

results, where the second error is again due to the systematic uncertainties.

The total cross section for photoproduction of J/ψ is shown in figure 4 together with earlier determinations in fixed target experiments at lower values of $W_{\gamma p}$ [1]. Our measurement is a factor $\sim 3 \pm 1$

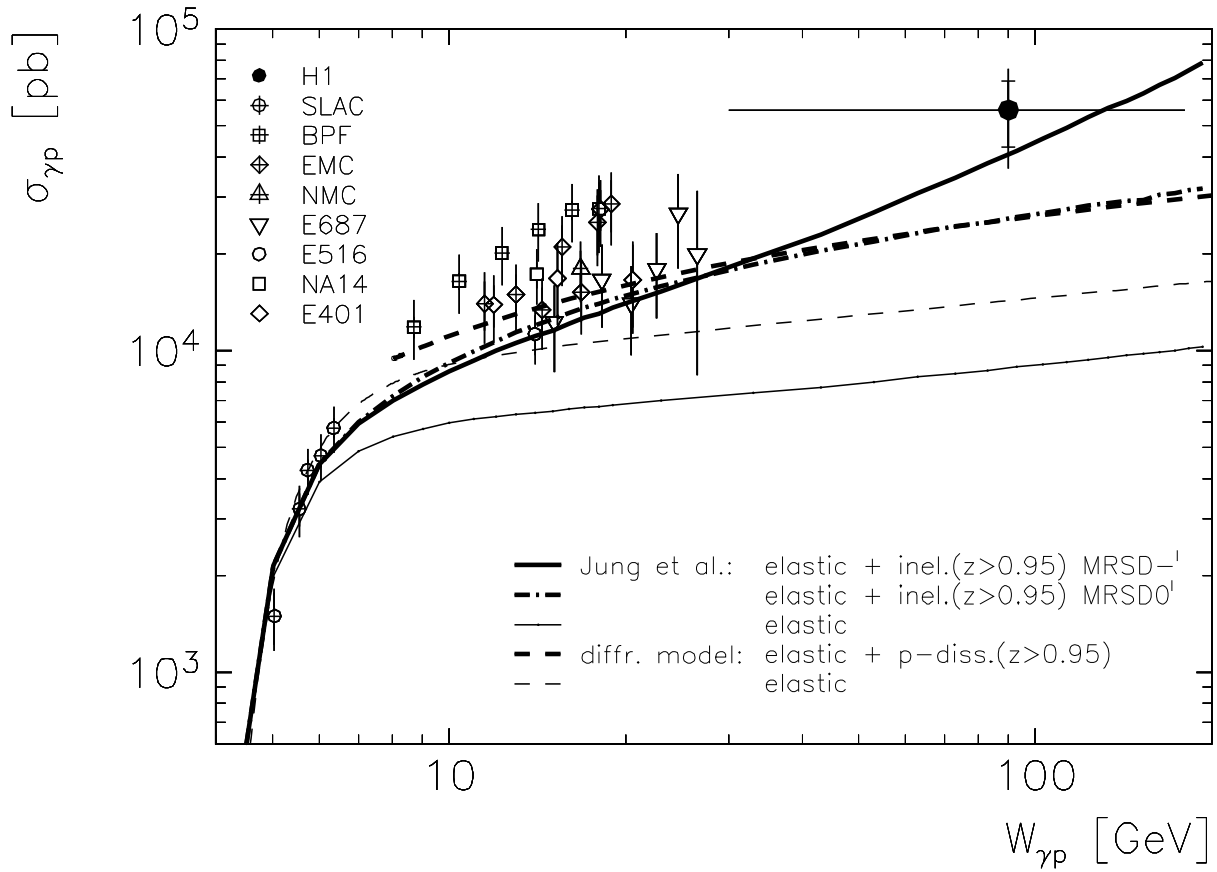


Figure 4: Total cross section for $\gamma p \rightarrow J/\psi + X$. The inner error bar of the H1 point is purely statistical, the outer one contains statistical and systematic errors added in quadrature. The horizontal error bar indicates the energy region covered. The data at lower center-of-mass energies are from previous experiments [1]; they were corrected with the new J/ψ decay branching ratio of [16] and include systematic errors (added in quadrature). The dashed curves show the predictions from the VMD model in PYTHIA [12], the thin dashed line is the elastic contribution only, the thick dashed line includes proton dissociation ($z > 0.95$). The thick full line shows the QCD model by Jung et al. [3] with the MRSD-’ parton density functions, the dash-dotted line with MRSD0’ (inelastic contribution for $z > 0.95$). The thin full line represents the purely elastic contribution in the QCD model.

above the data at $W_{\gamma p} \approx 20$ GeV, but caution is required in interpreting this figure. Since in our measurement nothing is known about the system ‘X’ in the final state the measured cross section contains contributions from elastic and inelastic diagrams, figures 1a and b in the VMD description or figures 1c and d in the QCD description. The inelastic contributions to the data can at this stage — lacking a separate measurement of either inelastic or elastic component — not be determined. Using the two models of inelastic J/ψ production one determines that our selection procedure accepts values of the elasticity parameter $z = E_{J/\psi}/E_\gamma \gtrsim 0.95$, where the energies are measured in the proton rest frame. This uncertainty about the composition of the data has been present to some extent in most previous experiments, which used different cuts to suppress inelastic contributions (e.g. the EMC Coll. applied a cut $z > 0.95$ [1]).

In figure 4 the data are also compared with model calculations, namely the VMD model implemented in PYTHIA [12] and the QCD inspired model by Jung et al. [3]. The VMD model is normalized to data at $W_{\gamma p} \approx 12$ GeV. The elastic contribution to the total rate at HERA energy is $\approx 50\%$ in this model. The expectation for elastic production derived by Jung et al. (compare diagram figure 1c) which uses the Pomeron form factor measured in proton-proton scattering [18] and splits

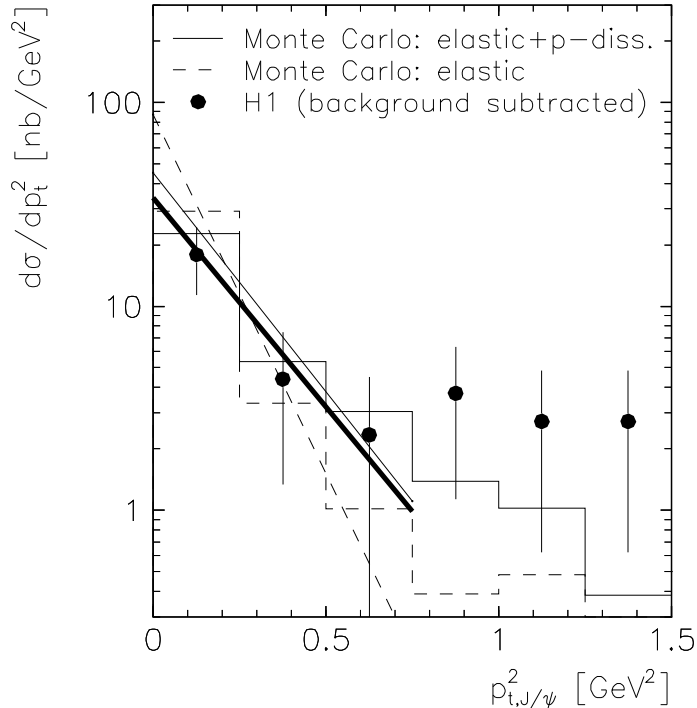


Figure 5: $d\sigma/dp_t^2$ for $ep \rightarrow J/\psi + X$ (QED background subtracted). The histograms show the PYTHIA Monte Carlo distribution: elastic plus proton dissociation (solid line), elastic contribution (dashed), the histograms are normalized to the measured ep cross section. The straight lines are exponential fits to the data (thick line), to the PYTHIA Monte Carlo (solid line) and to the elastic Monte Carlo distribution (dashed line).

the energy equally between the two gluons falls below the data at all energies above 10 GeV. If inelastic contributions with $z > 0.95$ are included, the improved colour-singlet model [3] using the MRSD-’ parton distributions [20] (thick full curve in figure 4) describes our measurement within one standard deviation (note that in [3] the colour-singlet model was normalized to inelastic data ($z < 0.8$) from EMC [19]). If a flat gluon distribution is chosen, e.g. MRSD0’ [20], the predicted cross section is lowered by a factor of 1.6 (figure 4). The MRSD-’ parton distributions are favoured by recent measurements of the proton structure function F_2 [21]. Since x_g -values $\gtrsim 10^{-3}$ contribute to J/ψ production the sensitivity to the gluon distribution is large.

In order to investigate the production characteristics the distribution of the momentum transfer t from proton to J/ψ was studied, where

$$t = (p_\gamma - p_{J/\psi})^2 \approx -p_{t,J/\psi}^2.$$

The latter approximation is valid for low Q^2 and small proton deflection angles. It is used as neither p_γ nor the momentum of the scattered proton are measured in the current apparatus. Figure 5 shows $d\sigma/dp_t^2$ for the J/ψ data sample. A fit to the data below $p_t^2 = 0.75$ GeV² (where the approximation for t is reasonable) yields a slope of $b = (4.7 \pm 1.9)$ GeV⁻². The error includes variations of the fit due to changes of the binning and of the p_t^2 -range used in the fit as well as systematic errors due to detector effects (± 0.4 GeV⁻²). The deviation from the exponential shape at larger values of p_t^2 is presumably due to contributions from events with finite values of Q^2 .

In a diffractive elastic model the slope parameter is expected to depend on the radius of the proton as $b = \frac{1}{2} < r_p^2 > \approx 8$ GeV⁻² if the small J/ψ -radius is neglected. For diffractive proton dissociation a less steep slope is expected [5]. The measured slope is small compared with the naive expectation

for elastic production. It is however consistent with measurements at lower center-of-mass energy which probably observed a similar mixture of elastic and inelastic production [1]. The exponential fits to the VMD model (figure 5) yield slopes of $b = (8.1 \pm 0.4) \text{ GeV}^{-2}$ for the elastic contribution but $b = (4.9 \pm 0.3) \text{ GeV}^{-2}$ for a mixture of 50 % elastic and 50 % proton dissociation. In the QCD inspired elastic model by Jung et al. [3] an effective slope of $b = 4.9 \text{ GeV}^{-2}$ results.

The distribution of the decay angle ϑ^* of the leptons in the J/ψ restframe was also studied since in all models helicity conservation at the photon J/ψ vertex is expected for $Q^2=0$ and hence a $1 + \cos^2 \vartheta^*$ distribution. The data are compatible with this hypothesis although due to limited statistics no significant limits can be placed on spin transition matrix elements.

The observed behaviour of the cross section and the p_t distribution of the J/ψ are consistent with a VMD production mechanism. Using the VMD relation $\sigma(\gamma p \rightarrow J/\psi p) = \frac{4\pi\alpha}{f_{J/\psi}^2} \cdot \sigma(J/\psi p \rightarrow J/\psi p)$ the cross section for elastic J/ψ proton scattering may be calculated; it is of the order of $100 \mu\text{b}$ if $f_{J/\psi}^2$ is calculated using the known mass and leptonic decay width of the J/ψ [16] and the relation $\Gamma_{\ell\ell}^{J/\psi} = \frac{\alpha^2}{3} \frac{4\pi}{f_{J/\psi}^2} \cdot M_{J/\psi}$. Again this cross section contains some unknown contribution from inelastic diffractive channels. Assuming a total cross section for J/ψ proton scattering of 1.4 mb , as was derived from EMC data in [22] for $W_{\gamma p} \approx 20 \text{ GeV}$, the elastic contribution is $\lesssim 7\%$, which is unusually small for a hadronic process and may be an indication for different scattering mechanisms of light and heavy flavours.

Conclusion

A first measurement of J/ψ meson production in electron proton collisions at $\langle W_{\gamma p} \rangle \approx 90 \text{ GeV}$ has been presented. Candidate events were selected via their leptonic decay and by requiring no additional particle in the detector besides the J/ψ candidate.

The measurement includes contributions from elastic and also from inelastic events where other particles are lost in the beampipe. The cross section for J/ψ photoproduction is compatible with a slow rise as extrapolated from low energy measurements taking into account some inelastic contribution. The data, in particular the exponential behaviour of the t -distribution, suggest that the dominant production mechanism is diffractive.

The QCD model describes the data reasonably well. The sensitivity to the gluon distribution in the proton is large but it is almost entirely due to inelastic contributions. Additional measurements are needed to disentangle elastic and inelastic contributions.

Acknowledgements

We are grateful to the HERA machine group whose outstanding efforts made this experiment possible. We appreciate the immense effort of the engineers and technicians who constructed and maintained the detector. We thank the funding agencies for financial support. We acknowledge the support of the DESY technical staff. We also wish to thank the DESY directorate for the hospitality extended to the non-DESY members of the collaboration.

References

- [1] U. Camerini et al., *Phys. Rev. Lett.* 35, 483 (1975)
- A.R. Clark et al., BPF Collaboration, *Phys. Rev. Lett.* 43, 187 (1979)
- J.J. Aubert et al., EMC Collaboration, *Nucl. Phys.* B213, 1 (1983)
- M. Arneodo et al., NMC Collaboration, *Phys. Lett.* B332, 195 (1994)
- P.L. Frabetti et al., E687 Collaboration, *Phys. Lett.* B316, 197 (1993)
- B.H. Denby et al., FTPS Collaboration, *Phys. Rev. Lett.* 52, 795 (1984)
- R. Barate et al., NA-14 Collaboration, *Z. Phys.* C33, 505 (1987)
- M. Binkley et al., E401 Collaboration, *Phys. Rev. Lett.* 48, 73 (1982)

- [2] J.J. Sakurai, *Ann. Phys.(NY)* 11, 1 (1960)
M. Gell-Mann, F. Zachariasen, *Phys. Rev.* 124, 953 (1961)
T.H. Bauer, R.D. Spital, D.R. Yennie, F.M. Pipkin, *Rev. Mod. Phys.* 50, 261 (1978)
S.D. Holmes, W. Lee, J.E. Wiss, *Ann. Rev. Nucl. Part. Sci.* 35, 397 (1985)
- [3] H. Jung D. Krücker, C. Greub, D. Wyler, *Z. Phys.* C60, 721 (1993)
- [4] E.L. Berger, D. Jones, *Phys. Rev.* D23, 1521 (1981)
- [5] K. Goulianos, *Phys. Rep.* 101, 169 (1983)
- [6] M. Derrick et al., ZEUS Collaboration, contributed paper 0672 to ICHEP94, 27th Int. Conf. on High Energy Physics, Glasgow, July 1994, to be published
S. Bhadra, Photoproduction and Diffraction at HERA, contribution to the Glasgow conference
C. Kleinwort, Studies of Charm Production with the H1 Detector, contribution to the Glasgow conference
- [7] I. Abt et al., H1 Collaboration, DESY preprint DESY 93-103 (1993)
(to be published in *Nucl. Instr. and Methods*)
- [8] J. Bürger et al., *Nucl. Instr. and Methods* A279, 217 (1989)
- [9] B. Andrieu et al., *Nucl. Instr. and Methods* A336, 460 (1993)
- [10] S. Eichenberger et al., *Nucl. Instr. and Methods* A323, 532 (1992)
- [11] Th. Wolff et al., *Nucl. Instr. and Methods* A323, 537 (1992)
- [12] T. Sjöstrand and M. Bengtsson, *Comp. Phys. Comm.* 43, 367 (1987)
H.U. Bengtsson and T. Sjöstrand, *Comp. Phys. Comm.* 46, 43 (1987)
- [13] V.M. Budnev et al., *Phys. Rep.* C15, 181 (1975)
- [14] F.W. Brasse et al., *Nucl. Phys.* B110, 413 (1976)
- [15] A. Suri and D.R. Yennie, *Ann. Phys. (NY)* 72, 243 (1972)
- [16] L. Montanet et al., Particle Data Group, *Phys. Rev.* D50, 1173 (1994)
- [17] H. Jung, G.A. Schuler and J. Terron, *Int. Journ. Mod. Phys.* A32, 7955 (1992)
- [18] K.H. Streng, in Proc. of the HERA Workshop, Vol. 1, p. 365, ed. R.D. Peccei, Hamburg 1987
- [19] J. Ashman et al., EMC Collaboration, *Z. Phys.* C56, 21 (1992)
- [20] A.D. Martin, R.G. Roberts and W.J. Stirling, *Phys. Lett.* B306, 145 (1993),
ibid. B309, 492 (1993)
- [21] I. Abt et al., H1 Collaboration, *Nucl. Phys.* B407, 515 (1993)
M. Derrick et al., ZEUS Collaboration, *Phys. Lett.* B316, 412 (1993)
- [22] F.D. Gault and A.B. Rimmer, *Nuovo Cim.* 74A, 1 (1983)